


 Cite this: *Lab Chip*, 2017, 17, 1349

Microfluidic continuum sorting of sub-populations of tumor cells *via* surface antibody expression levels†

 Rhonda Jack,^a Khadijah Hussain,^b Danika Rodrigues,^c Mina Zeinali,^{af} Ebrahim Azizi,^d Max Wicha,^d Diane M. Simeone^e and Sunitha Nagrath^{*a}

The extent of inter- and intra-tumor cell heterogeneity observed in patient tumors appears to be directly associated with patient prognosis. Moreover, studies indicate that targeting distinct subpopulations of tumor cells may be more relevant to successfully managing cancer metastasis. The ability to distinguish and characterize unique tumor cell subpopulations within a given sample is thus exigent. Existing platforms separate cells binarily, based on some threshold level of phenotypic characteristics without consideration of the continuum levels of biomarker expression and the associated implications. Herein we describe how specific tumor cell groups have been immunomagnetically enriched according to a continuum of EpCAM surface marker expression levels. Even among a relatively homogenous group of cells such as the PANC-1 cell line, cells could be separated according to their EpCAM levels into low, moderate and high expression. To physiologically assess each subpopulation, a wound healing assay was performed which revealed distinct invasive potentials among each subset. Furthermore, the clinical relevance of the approach was demonstrated by isolating pancreatic cancer CTCs from the same patient sample based on their EpCAM levels. We demonstrate a robust method of isolating CTCs according to their varying protein levels, which enables extensive studies on tumor cell heterogeneity. Interestingly, 5 of 6 samples had CTCs that could be recovered at all three levels of EpCAM expression though the majority of CTCs were recovered as low expression events. Preliminary studies that compare tumor cell subpopulations in this continuum manner can potentially increase our understanding of the dynamic nature of cell heterogeneity and how it relates to patient outcomes. Ultimately further investigation may yield therapeutic targets against virulent cell subpopulations.

 Received 6th December 2016,
Accepted 3rd March 2017

DOI: 10.1039/c6lc01496h

rsc.li/loc

Introduction

The clinical ramifications of tumor heterogeneity have been demonstrated in a number of studies that investigate the levels of heterogeneity among patients and how these levels correlate with patient outcomes.^{1–3} It is believed that genetically distinct subclones that comprise tumors cooperate to facilitate tumor growth and progression and as such, tumor

heterogeneity is thought to be necessary for sustained tumor growth progression.^{4,5} Identifying the heterogeneous populations of cells that comprise tumors has influenced decisions in patient treatment as interpatient tumor heterogeneity provides a platform for molecular biomarker testing and predictions of patient response.⁶ Moreover observations that such biomarkers may evolve over the clinical course, has led to increasing focus on the impact of intratumor heterogeneity in patients.⁶ In light of the significance that tumor heterogeneity plays, whether among different patients or within a single tumor from a patient, the need to sensitively and reproducibly interrogate tumor heterogeneity is imminent.

Furthermore, a small subset of tumor cells is thought to be responsible for the metastatic cascade in many solid tumors.^{7,8} These cells acquire the ability to disseminate from the tumor and travel through the vasculature before initiating a secondary tumor at another site, demonstrating biological properties that are distinct and crucial to metastasis. Circulating tumor cells, (CTCs) represent prime targets in the fight against metastasis. Therefore the ability to isolate and

^a Department of Chemical Engineering, University of Michigan, 2300 Hayward St, Ann Arbor, MI 48109, USA. E-mail: snagrath@umich.edu

^b Department of Cell and Developmental Biology, University of Michigan, 109 Zina Pitcher Pl, Ann Arbor, MI 48109, USA

^c Department of Biomedical Engineering, University of Michigan, 2200 Bonisteel Ave, Ann Arbor, MI 48109, USA

^d Comprehensive Cancer Center, University of Michigan Health Systems, 1500 E. Medical Center Dr, Ann Arbor, MI 48109, USA

^e Department of Surgery, University of Michigan Health Systems, 1500 E. Medical Center Dr, Ann Arbor, MI 48109, USA

^f Institute for Medical Technology of Heidelberg University & University of Applied Sciences Mannheim, Mannheim, Germany

† Electronic supplementary information (ESI) available. See DOI: 10.1039/c6lc01496h

interrogate these different subtypes can potentially open many clinically beneficial avenues towards cancer management.^{9,10}

One approach that has been adopted for tumor cell sorting is performing fluorescently activated cell sorting (FACS) on tumor cells that have been digested from tumor tissue or tumor derived cell lines.^{11,12} FACS has been universally employed for sorting cell subpopulations as it conveniently allows rapid cell measurement readouts of 10^4 cells per s. Additionally the limit of detection of 1 fluorescent cell is 10^{-6} and multiple cell surface markers can be analysed simultaneously. Typically cells are sorted according to high and low levels of surface markers of interest based on their fluorescence intensity where most studies to date gate and separate cell subpopulations based on very high (positive) and very low (negative) expression of proteins of interest. Thus cell sorting is carried out without considering the continuum levels of phenotypic characteristics and their associated implications with respect to tumor cell heterogeneity. Apart from its costliness, FACS sorting becomes less advantageous when small numbers of cells are considered as is often the case with rare CTCs from patient samples. Using FACS to sort the few CTC events that occur among billions of other blood cells represents a less sensitive approach that can potentially become time consuming and impractical.^{8,13,14}

To sort cells according to their varying levels of surface marker expression one study reported development of a

nanoparticle mediated microfluidic cell sorting approach that used velocity valleys to slow and trap cells.¹⁵ Purities were 19% when target cells were trapped from blood and overall throughput was 2 mL h^{-1} .¹⁵ Currently, the majority of molecular assays that are performed subsequent to CTC isolation necessitate high purities so that molecular profiling and analysis that is specific to CTCs can be obtained. Previously, we demonstrated highly sensitive and robust CTC isolation through size-based inertial pre-sorting of whole blood followed by immunomagnetic CTC labeling and magnetic CTC sorting using the integrated microfluidic magnetic cell sorting system (see Fig. 1B). The method allowed for 100% of rare CTC detection and isolation in among a cohort of 14 cancer patients.¹⁶

By implementing simple alterations and a strategic workflow to the magnetic sorter module (Fig. 1B and C), we demonstrate the ability to isolate distinct groups of tumor cells immunomagnetically, according to their levels of surface protein expression. Essentially the magnetic field strength experienced by magnetic particles under flow in the microfluidic channel was manipulated by meticulously adjusting the distance of the external magnet from magnetic particles flowing in the sorter. As a result cancer cells that were immunomagnetically labelled with $1 \mu\text{m}$ magnetic beads were sorted based on their different levels of magnetic bead attachment among them. We demonstrate that even with magnetically labelled cells that occur at a low frequency

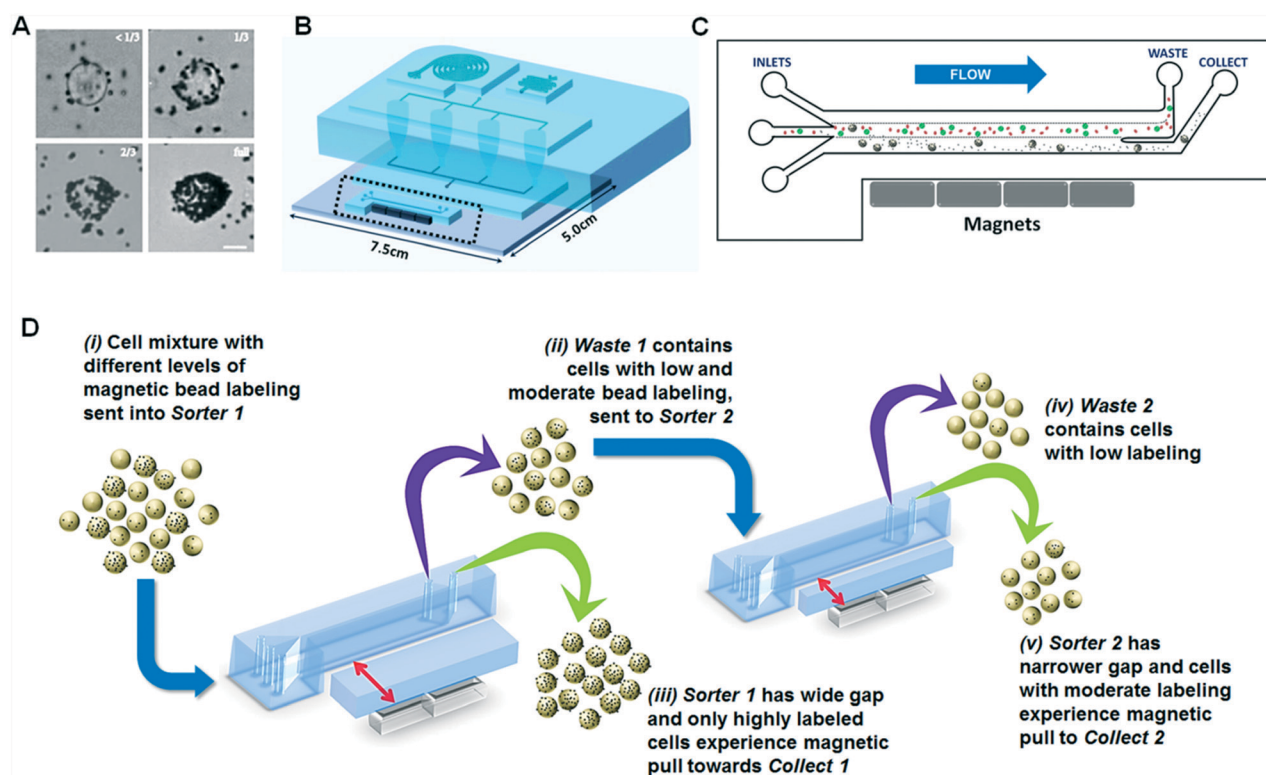


Fig. 1 Magnetic sorter module (A) bead attachment categories used to evaluate cell-magnetic bead coverage (scale bar represents $10 \mu\text{m}$). (B) Magnetic sorter module outlined in illustration of the integrated magnetic cell sorting platform (C) schematic of magnetic sorter outlets used to collect magnetized cancer cells. (D) Schematic of 2-tier magnetic sorting process used to isolate 3 cell populations based on low, moderate and high levels of protein expression. Red arrows indicate separation width between sorter and external magnet.

among non-target cells, this approach can be applied in their isolation. In addition, the clinical utility of the device was demonstrated by processing pancreatic ductal adenocarcinoma (PDAC) blood samples from 6 patients and characterizing the isolated CTCs from these samples. Tumor cells were isolated based on low, moderate and high EpCAM levels and were studied and compared to determine any detectable differences such as detection rate, and morphological features.

Material and methods

PDMS microfluidic chip fabrication

Microfluidic channels were designed using AutoCAD and master molds were fabricated using SU8-100 negative photoresist (Microchem Corp.) following standard photolithography procedures. All molds were fabricated with a thickness of 100 μm . A 10:1 ratio of PDMS polymer to curing agent (Dow-Corning) was mixed and de-bubbled prior to pouring over the SU8 molds. The PDMS was allowed to cure at 65 $^{\circ}\text{C}$ overnight. After curing, the PDMS chips were manually cut and peeled from the mold, cut to size, and inlet/outlet holes were punched. PDMS chips were bonded by oxygen plasma to pre-cleaned glass slides. Tygon tubing was inserted to connect device inlet and outlet ports with syringes. All flow was controlled and driven by automated Harvard Apparatus syringe pumps. Prior to running samples, tubing and chips were flushed and primed with 1% Pluronic F127 solution followed by PBS for several minutes to prevent sample components from adhering to the PDMS surfaces of the devices.

Cancer cells

PANC-1 cells (human pancreatic carcinoma, epithelial-like cell line), obtained from ATCC, were maintained at 37 $^{\circ}\text{C}$ in 5% CO_2 and 95% relative humidity in DMEM, supplemented with 10% FBS. Cells were harvested on the third day after seeding, once they achieved >60% confluence, to exploit optimal cell surface EpCAM expression. For appropriate dilutions, cells were counted using a hemocytometer and then diluted with PBS accordingly. For labeling cells with EpCAM-coated magnetic beads, cells were diluted in PBS buffer and incubated with diluted magnetic beads at a 10:1 volume ratio for <1 h. For cells that were fixed, 4% PFA was used. Fixed cells were stored at 4 $^{\circ}\text{C}$ whenever necessary.

FACS sorting

Cells processed through the magnetic sorter were resuspended in 3% BSA and allowed to incubate on ice for 15 min. Samples were diluted to 1% BSA and FACS dye (R&D Systems Human EpCAM/TROP-1 Alexa Fluor 488-conjugated monoclonal mouse IgG2B antibody) was added to the sample and allowed to incubate for 20 min. Sample were rinsed with PBS and fixed with 4% PFA. FACS was carried out on the samples using MoFlo Astrios EQ FACS platform (Beckman Coulter) while gating and data collection was done using the

Summit6.3 software. Data post-processing and analysis was done with FlowJo v.10 software.

Human blood sample collection and processing

Blood samples from pancreatic cancer patients were collected using institutional IRB guidelines with informed consent from the patients or the next of kin. The patient samples, (courtesy of the University of Michigan Comprehensive Cancer Center) were collected in EDTA tubes and tested within six hours of blood draw. For each sample, 5 mL of whole blood was processed through the integrated microfluidic device.

Immunofluorescence staining of isolated CTCs

CTCs isolated by the integrated device were processed by cytospinning 250 μL of sample and then fixing with 250 μL of 4% PFA for 20 min. Slides were then stained for CTC markers using a primary antibody for anti-cytokeratin-19 (CK-19), and for anti-pan cytokeratin (pan-CK) epithelial cell markers, (Santa Cruz Biotechnology, rabbit polyclonal IgG), as well as nuclear stain 4',6-diamidino-2-phenylindole, dihydrochloride (DAPI, Invitrogen). Negative staining with the leukocyte marker anti-CD45 (BD Pharmingen Purified Mouse Anti-Human CD45, HI30 clone, isotype Mouse IgG1, κ) was also performed. Samples were then stained using secondary antibodies with fluorescence conjugation namely, AlexaFluor 568 (Life Technologies), for CK-19 detection and AlexaFluor 488 (Life Technologies), for CD45 detection. For the primary antibody stains, an overnight incubation period was carried out, while for secondary staining, 1 h was allowed. For DAPI staining ProLong Gold antifade mountant with DAPI, (Life Technologies) was applied overnight. Immunofluorescence imaging for anti-CD45 was performed using a FITC filter while anti-CK was performed with a PE filter and DAPI, a UV filter. Based on immunofluorescence imaging and analysis, a CTC should be positive for CK and DAPI, while demonstrating no signal for CD45.

Evaluating cancer cell line surface-protein levels

The feasibility of the immunomagnetic continuum sorting concept is predicated on heterogeneity in surface protein expression levels among the target cell. Thus we evaluated the differences in surface protein expression levels of cells within the same cell line passage to establish the practicality of the approach. EpCAM protein expression was studied since EpCAM is widely expressed among CTCs and is extensively used as the CTC capture antibody.¹⁷ Additionally, the pancreatic adenocarcinoma PANC-1 cell line was selected as a relevant reference alongside the PDAC patient samples that were included in the study. To characterize the levels of EpCAM on PANC-1 cells, it was assumed that for viable cancer cells that are mixed and incubated with an excess of antibody-coated, magnetic microbeads, the quantity of magnetic bead attachment to a cell indicates the available protein on the cell surface, provided that neither incubation time nor bead

availability are limiting factors. PANC-1 cells were incubated with magnetic beads for 5, 10, 15 and 30 min and then immediately imaged for the level of bead coverage on the cells. After 30 min, there was negligible increase in cell bead coverage compared to the 15 min incubation period indicating that the time range tested for incubation periods was sufficient. Each cell was categorized as having a surface coverage level of magnetic beads of either none, $<1/3$ (low), $1/3$ to $2/3$ (moderate) or $>2/3$, (high) coverage (see Fig. 1A).

Results and discussion

As seen in ESI† Fig. S1, even after 30 min of incubation, almost 3% of PANC-1 cells still maintained $<1/3$ bead coverage, thus indicating a relatively negligible EpCAM expression among those cells. 8% of cells had $>2/3$ bead coverage, indicating high expression levels of EpCAM in this subset of cells. MiaPACA-2 cells which are known to express low EpCAM levels were tested as a control, using the same procedure. For MiaPaca-2 cells, as much as 64% of cells showed $<1/3$ EpCAM bead coverage after 30 min of incubation. Based on these results from magnetic bead attachment, PANC-1 cancer cells from the same passage, which are relatively homogeneous compared to tumor cells in circulation, demonstrate different levels of protein expression. In turn this indicates the heterogeneity that exists among cells within the same tumor and points to the possibility of sorting cells according to some continuum of surface protein expression level.

Magnetic sorter module

The magnetic sorting module is part of the previously reported integrated microfluidic immunomagnetic device shown in Fig. 1B.¹⁶ The device was implemented to isolate rare CTCs from whole blood with high sensitivity and CTC purity rates, at a high sample throughput. The blood sample is first presorted at 24 mL h^{-1} to reduce erythrocyte and leucocyte contaminants after which the sample mixes with magnetic beads on chip, followed by immunomagnetic sorting of magnetically labeled CTCs. Typically, the resulting sample is a significantly enriched suspension of CTCs.¹⁶ Based on the continuum of protein expression displayed by cells from the same passage the next step was to determine whether the magnetic sorter module (outlined in Fig. 1B) could be leveraged to effectively separate cell subpopulations based on incremental differences in protein expression. Fig. 1C shows that for a cell suspension under flow in the magnetic sorter, an external magnet which is placed parallel to the main sorter channel attracts only magnetized cells to the collection outlet with high purities by separating them away from unlabelled cells.

We hypothesized that by adjusting the separation distance on the micron scale between the flowing cell suspension and the magnet, the magnetic field strength experienced by the magnetized cancer cells could be tuned. In so doing, the magnetic force experienced by subsets of cells, dependent on their varying levels of magnetic bead coverage, could be tuned and

so cells could be separated according to their levels of protein expression. Fig. 1D illustrates the approach we hypothesized to separate cells from the same cell suspension according to low, moderate and high levels of EpCAM expression. For a wide separation gap only cells with very high magnetic bead attachment would experience a magnetic force strong enough to separate them from the flowing cell suspension. The effluent waste of the first magnetic sorter, now depleted of cells with high magnetic bead coverage would then be processed through a magnetic sorter with a narrower separation gap so that cells having moderate bead attachment would be separated from the rest of cells into the collection stream. Ideally, the effluent waste of the second magnetic sorter, now depleted of cells with moderate bead coverage would contain cells having low to no bead attachment. Therefore cells from the same population would be separated according to low, moderate and high EpCAM levels.

Tuning magnetic flux density

The magnetic flux profile in Fig. 2A, generated in COMSOL, shows the variation of magnetic flux densities developed by a single magnetic bead in the microfluidic channel, positioned at either the near edge (blue line) or far edge (black line) of the magnetic sorter where “near” and “far” represent distances from the magnet. Since the magnetic flux density decreases with increasing distance from the magnetic source, adjusting the distance between the magnetic particle and the external magnetic source alters the strength of the magnetic force experienced by the magnetized particle. Additionally, the intensity of the magnetic force is dependent on the magnetization of the magnetic particle, which correlates with the number of beads attached to each cell. By tuning the strength of the magnetic force developed *via* adjustment of the gap distance, cells having low, moderate and high magnetic bead coverage and therefore expressing low, moderate and high EpCAM levels, respectively, could be isolated individually.

Fig. 2B shows the distribution of flowing cells in the magnetic sorter. As indicated by the rightmost arrow, the largest vertical distance across the channel width a magnetized cell needs to traverse to be pulled into the collection channel, L_y , is $150 \mu\text{m}$. In the absence of beads or a magnet, and with sample input flow set at $50 \mu\text{L min}^{-1}$, cells were tracked under a high speed camera in laminar flow through the microchannel. By particle tracking, the linear velocity in the x -direction (u_x) was determined to be 125 mm s^{-1} . So for a channel length, $L_x = 25 \text{ mm}$ in the direction of flow, the time that a cell is exposed to the magnetic field, or its residence time, t_r was determined to be 0.2 s. Based on these calculations, it is implied that a cell needs to travel a vertical distance of $150 \mu\text{m}$ in 0.2 s. Consequently, for $t_r = 0.2 \text{ s}$ and $L_y = 150 \mu\text{m}$, the minimum vertical traversing velocity, u_y , of the cell to successfully enter the collection channel is $750 \mu\text{m s}^{-1}$. Achieving this velocity is dependent on cells having sufficient magnetic bead attachment to experience a sufficient magnetic force, F_M , to magnetically pull them towards the collection channel. The minimum required bead

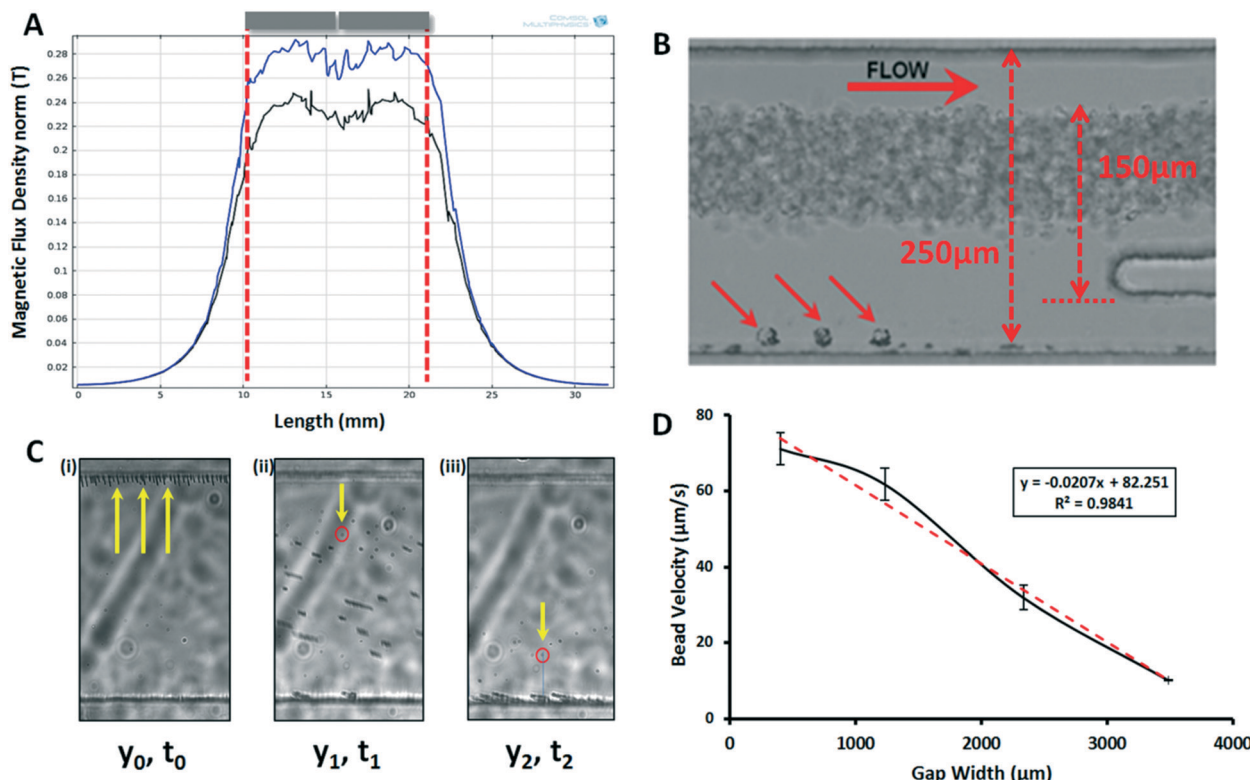


Fig. 2 Controlling particle magnetic force (A) COMSOL simulation of magnetic flux density at the near edge (blue line) and far edge (black line) of the channel in relation to the external magnets (B) cell distribution under laminar flow in the magnetic sorter channel module and device measurements (C) tracking a single magnetic bead to determine bead velocity (D) plot shows how bead velocity varies as a function of gap distance between magnet and channel. Cell with relatively high bead coverage can be magnetically collected while cells having fewer beads remain in the waste stream. Thus cells from the same sample could be separated using the system according to levels of low, medium and high protein expression (red broken line indicates best fit line of plot).

attachment for a cell in turn, is dependent on the separation width, such that as distance increases, the minimum number of beads required increases.

To determine how the magnetic sorter separator width affected the minimum bead coverage required for a cell to be deflected and separated into the collection channel, four different separator widths, (400, 1200, 2300 and 3400 μm) were studied. For a superparamagnetic microparticle exposed to a magnetic field range that saturates its magnetization, velocities are proportional to the magnetic field gradient.^{18–20} Assuming electrostatic and van der Waals forces are negligible and the magnetic force F_M dominates, the drag force acting on the particle balances F_M and so Stokes law can be applied.^{18,19} Thus, under laminar flow, the magnetic force can be approximated such that,

$$3\pi\eta u_t D_{\text{bead}} = F_{D\text{bead}} = F_{M\text{bead}} \quad (1)$$

where η is the fluid viscosity, u_t is the terminal velocity in the direction perpendicular to flow (which was approximated by tracking bead movement across the channel), D_{bead} is particle diameter, and F_D is the drag force.^{18,19}

By the same token, for a magnetized cell,

$$3\pi\eta u_t D_{\text{cell}} = F_{D\text{cell}} = F_{M\text{cell}} \quad (2)$$

Given that each bead attached to a cell contributes equally to the total $F_{M\text{cell}}$, F_M of the total number of beads is taken to be equal in magnitude to cell magnetic force and thus the cell drag force, $F_{D\text{cell}}$. Moreover, the minimum magnetic bead attachment required by a magnetized cell for it to be deflected to the collection channel was determined by the magnetic force required to achieve a cell velocity of $750 \mu\text{m s}^{-1}$.

For the magnetic beads, the only unknown, u_t was estimated by tracking and measuring the movement of a single magnetic bead in the microfluidic channel as demonstrated in Fig. 2C. In Fig. 2C(i), y_0, t_0 corresponds to initial bead position at time 0 s while y_1 and t_1 correspond to positions 1 at time t_1 , and y_2 corresponds to position 2 at time t_2 . For each width, to determine the velocities of the particles, initially, magnetic beads were placed into the microfluidic channel and directed, magnetically to the channel edge further away from the designated position of the permanent magnet, at y_0, t_0 . Then the permanent magnet was positioned at the designated gap distance and the movement of particles towards the permanent magnet, from y_1 at time t_1 to y_2 at t_2 was recorded at a rate of 50 frames-per-second (fps) rate using a high speed camera. For each gap width, the velocity of a single magnetic bead, $u_t = u_{y(\text{bead})}$ was determined based on these values.

For N number of beads attached to a cell,

$$F_{\text{Mcell}} = [N \times F_{\text{Mbead}}] \quad (3)$$

By Stokes law,

$$[D_{\text{cell}} \times u_{y\text{cell}}] = [N \times D_{\text{bead}} \times u_{y\text{bead}}] \quad (4)$$

Recalling that the minimum required bead velocity for successful deflection is $750 \mu\text{m s}^{-1}$ and taking cell diameter as $20 \mu\text{m}$, for $1 \mu\text{m}$ beads,

$$N = [20 \mu\text{m} \times 750 \mu\text{m s}^{-1}] / [D_{\text{bead}} \times u_{y\text{bead}}] \quad (5)$$

Fig. 2D shows how bead velocity, u_y , varies with gap widths. This in turn affects the minimum number of beads required for cells to be sorted successfully given the sorter dimensions and sample flow rate of $50 \mu\text{L min}^{-1}$. For instance based on such calculations, by using the velocities ($u_{y\text{beads}}$), reported in Fig. 2D and eqn (5), results in Fig. 3A show that with a gap size increase from 400 to $1200 \mu\text{m}$, the minimum number of beads, N , required increased by 1.2 fold while an

increase to $3400 \mu\text{m}$ required 7 fold increase in the minimum required number of beads. Overall, it can be seen that at sufficiently large of a gap size, only those cells having relatively high bead coverage can be magnetically deflected while cells having fewer beads remain in the waste stream. Based on these results, cells from the same sample could be separated using the continuous sorting system according to levels of low, medium and high protein expression.

Developing a cell separation workflow

Considering the proposed workflow for separating cells according to their continuum level of EpCAM expression (Fig. 1D), two different magnetic sorter gap widths, one narrower and one wider, were required for continuum cell sorting. To determine the most effective 2-sorter combination of widths that would facilitate isolation of relatively low, moderate and high EpCAM expressing cells, the four magnetic sorters of different gap sizes were tested with magnetic bead-labeled cancer cells. This range of widths (400–3400

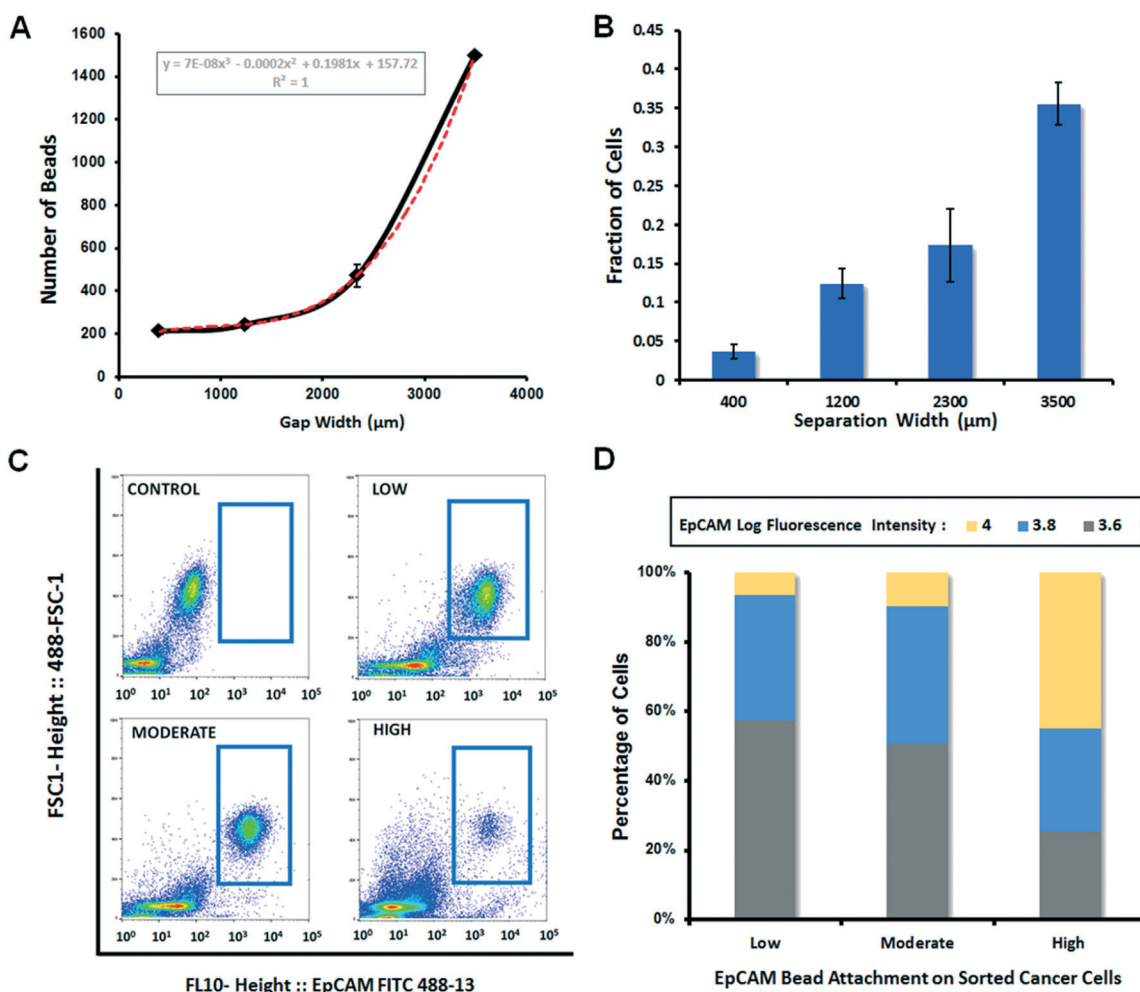


Fig. 3 Tuning magnetic force to sensitively isolate cell subpopulations (A) effect of magnetic sorter gap width on required number of beads attached to cell for magnetic isolation (red broken line indicates best fit line of plot). (B) Effect of gap width on isolation of cells with full magnetic bead coverage. (C) FACS dot plots and (D) FACS histogram of EpCAM protein detected from PANC-1 cells isolated according to low, moderate and high EpCAM protein expression.

μm) was specifically selected to avoid magnetic bead build-up in the channel. Bead buildup or accumulation occurs with gaps that are too narrow, which leads to beads becoming entirely immobilized within the channel by the magnetic force. Additionally, the range was selected to avoid too weak of a magnetic field strength with gaps so wide that no magnetic particles or cells get magnetically deflected to the collection outlet. Firstly, each sorter was tested individually to evaluate the bead attachment on the cells isolated in both waste and collection channels of the sorter. A cell suspension was prepared at a spiking rate of 10^3 cells per mL from PANC-1 cells that were labelled with EpCAM conjugated magnetic beads. Based on previous flow rate optimization with the magnetic sorter module, 1 mL of the suspension was driven through the sorter at $50 \mu\text{L min}^{-1}$ with the upper and lower buffer streams flowing at 25 and $75 \mu\text{L min}^{-1}$ respectively. To evaluate and compare the ability of the devices to effectively sort magnetically labelled cells, the bead attachment of cells in the collection and waste outlets were analysed.

As seen in Fig. 3A, among the collection samples of the four sorters, as the gap size increased there was an increase in the percentage of cells appearing fully covered with magnetic beads. Additionally, as the gap size increased there appeared to be a tradeoff between the percentage of cells having full coverage and the percentage recoveries of cells with $>2/3$ bead coverage where percentage recoveries declined as gap size increased from 1200 to 2300 to $3400 \mu\text{m}$ (Fig. S2†). This may indicate that cells with fairly high bead coverage ($>2/3$) are not sufficiently magnetized to be recovered as the magnetic separation distance increases above $1200 \mu\text{m}$. Fully covered cells however, appear to be sufficiently magnetized to be magnetically recovered as the magnetic separation distance increases (see Fig. 3B). Based on these results, gap widths of $1200 \mu\text{m}$ and $2300 \mu\text{m}$ were selected for the 2-sorter separation workflow since both devices had high recovery rates. Also there is a significant increase in the fraction of cells having extremely high EpCAM expression (fully covered cells) sorted from the $2300 \mu\text{m}$ gap compared to the $1200 \mu\text{m}$ gap. This increase indicates that the $2300 \mu\text{m}$ sorter would be able to sort the majority of high EpCAM expressing cells. The workflow adopted to sort cells in a continuum manner involved initial cell sorting through a sorter with $\sim 2300 \mu\text{m}$ gap to collect high EpCAM expressing cells followed by cell sorting of the waste outlet through a sorter with $\sim 1200 \mu\text{m}$ gap to collect moderate EpCAM expressing cells from the collection outlet and low EpCAM expressing cells from the waste.

To evaluate the effectiveness of the 2-sorter separation strategy to sort cancer cells according to low, moderate and high EpCAM levels from the different sorter combinations, magnetically labeled cancer cells (10^4 cells per mL) were processed using the decided workflow. Then FACS analysis was performed to determine the level of EpCAM on the magnetically separated cell subsets. FACS dot plots of particle size (FSC-1 height) versus particle fluorescence intensity (EpCAM log FL10 height) for control unstained cells and for cells anticipated to have low, moderate and high protein expres-

sion are shown in Fig. 3C. The samples are gated based on their relative fluorescent EpCAM intensity compared to the unstained control. To better quantitate and compare the relative levels of EpCAM in each of the magnetically sorted populations, cell fluorescent intensities from FACS readouts (FL10 height) were analyzed using Flowjo software. As seen in the histogram plot in Fig. 3D, the fraction of cells expressing the highest EpCAM fluorescence of log FL10 height of ≥ 4 increased in moving from cell subsets sorted according to low ($n = 1636$), to moderate ($n = 693$), to high ($n = 406$) EpCAM expression, while there was a decrease in the fraction of cells with lowest EpCAM expression at log FL10 height of ≥ 3.6 . Thus FACS analysis on the samples supports the hypothesized approach of sorting cells according to a continuum of EpCAM expression.

Scratch assay of cell subpopulations

Traditionally scratch assays have been employed to investigate the relative proliferation and migrations rates of mammalian cells, which in turn could be extrapolated to the invasive potential of cells.^{21,22} To investigate whether the samples sorted according to varied EpCAM protein levels would display unique physiological differences beyond surface EpCAM expression, a scratch assay was carried out on the three cell subsets. A control population that was not processed through the magnetic sorters was also investigated for comparison. To conduct the scratch assay, 3 mL of a sample containing viable, EpCAM-bead labelled PANC-1 cells was processed through the $2300 \mu\text{m}$ magnetic sorter gap and the collection effluent was designated as high expression. Then the waste effluent from this sorter was processed through the $1200 \mu\text{m}$ magnetic sorter. The effluent of the collection channel from this second sorter was designated moderate expression while the waste channel was designated low expressing cells. Once low, moderate and high expressing cells were collected, the cell densities in each well were determined and adjusted by resuspending so that a comparable cell density could be achieved. Each cell subpopulation was then plated and complete media was added to each culture plate to allow cells to grow. Additionally, EpCAM-bead labelled cells from the same cell line passage were plated at a comparable cell density to the other plated wells to use as a control (see Fig. 4A).

To perform the scratch, for each well, once 80% confluence was achieved in the well, a scratch was performed using a micropipette tip on day 0, and the healing rate of the scratch was monitored by capturing images of each well on day 1 and then each day until the scratch healed (see Fig. 4B). By measuring the rate at which the scratch was repopulated with new cell growth over the cleared surfaced for each sample, the invasive potential among the samples could be compared. For each scratch on each day, three measures of the scratch width were taken and the average width was recorded. Additionally to investigate whether cells would maintain these relative EpCAM expression levels after sorting, cells sorted according to the continuum approach of low

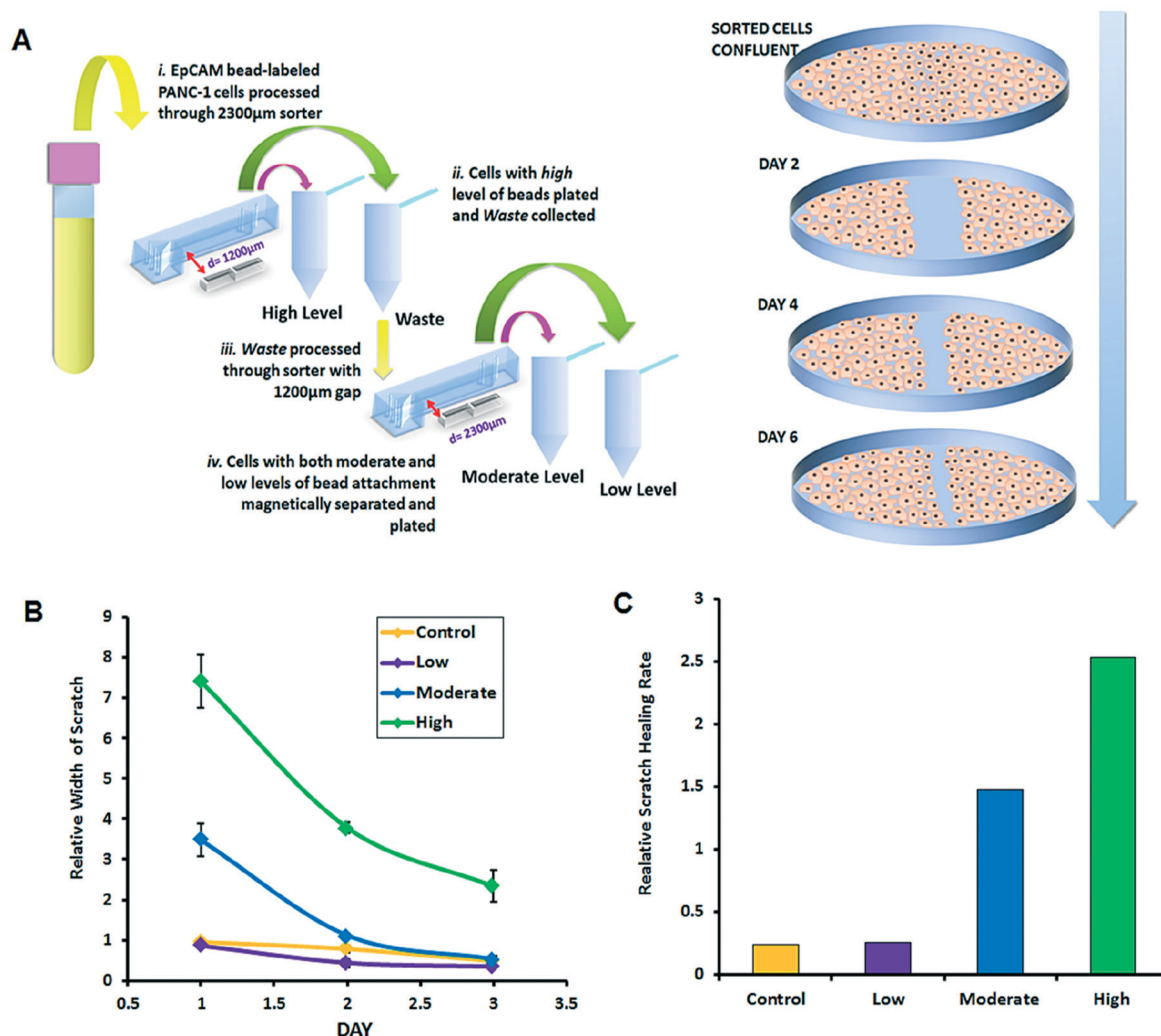


Fig. 4 Tumor cell scratch assay of low, moderate and high EpCAM levels (A) schematic of process used for isolating cells according to 3 varying levels of EpCAM and performing scratch assay with isolated cells (arrow indicates time progression from day 0 to time of scratch healing). (B) Relative scratch widths for low, moderate and high levels of EpCAM and an unprocessed control (C) relative healing rates for different cell subpopulations determined by gradient of best fit line from rates in (B).

moderate and high EpCAM expression were cultured for six days. On day six cells were relabelled with EpCAM beads. Fig. S3[†] shows that even after six days of culturing, cells appear to maintain the same relative EpCAM expression levels.

In determining the scratch healing rate for each sample, normalization was conducted based on the initial cell density recorded immediately after plating each sample. Cell density was divided by the change in scratch width for each condition, each day and plotted as a function of time. Fig. 4B shows these relative or normalized scratch widths for the control, low, moderate and high EpCAM levels. Discrepancies in day 1 relative widths reflect different cell densities as well as differences in the initial widths inscribed by the pipette tips among the four conditions. Estimates of the relative scratch healing rate, taken as the negative slope of the plots in Fig. 4B, were compared among the four conditions. As seen in Fig. 4C the level of EpCAM expression on cell subpopulations appears

to directly correlate with the scratch healing rate such that, as the level of EpCAM increases, the scratch healing rate also increases. The control population of cells appears to heal at a comparable rate to cells isolated according to low protein levels.

While the bio-physiological basis for these results needs to be further investigated, results demonstrate that the continuum sorting approach was able to separate cell subpopulations that display unique motility rates after being cultured.

Continuum isolation of PDAC patient derived CTCs

To determine whether a similar isolation approach could be useful in the context of patient derived CTCs, blood samples collected from six PDAC patients were analysed using the continuum isolation approach. For each patient 5 mLs of whole blood was pre-sorted using the inertial spiral sorter of

the previously reported integrated microfluidic system.¹⁶ The effluent of the spiral was then directly mixed with EpCAM magnetic beads on chip *via* the passive mixer and the mixture was allowed to incubate for 20 minutes. The sample was then processed using the workflow described here to sort the CTCs according to low, moderate and high levels of EpCAM. CTCs were identified as cells staining positive for nuclear content with DAPI and being panCK⁺ or CK19⁺/CD45⁻. In most instances, EpCAM bead labeling served as an additional means of identifying epithelial derived CTCs. As seen in Fig. 5A, the majority of CTCs appear to express low levels of EpCAM among the 6 patients (mean = 66.2% ± 23.45) compared to moderate (mean = 12.9% ± 11.87) or high (mean = 20.9% ± 20.23) expression levels. Fig. 5B shows brightfield and immunofluorescent images of CTCs isolated based on low, moderate and high EpCAM expression levels. Especially with brightfield imaging, the heterogeneity among CTC EpCAM expression can be readily observed. These results point to the potential of the approach described to discriminate among different CTC subpopulations according to their surface protein expression levels.

Conclusion

Numerous reports so far have described probable mechanisms of cancer metastasis and how distinct cell subpopulations comprising tumors uniquely contribute to the invasive metastasis cascade. Therefore platforms to separate tumor cells according to their different subpopulations are crucial. Most studies characterize tumor cells according to positive and negative expression of proteins of interest without consideration of low, moderate and high expression of protein levels. Here we report isolation of pancreatic tumor cells according to low moderate and high levels of EpCAM protein. FACS analysis on the samples corroborated the ability of the described approach to sort cells according to their varying EpCAM expression levels. Additionally, characterization of tumor cells according to such categories revealed notable differences among the three groups based on their invasive potential. Furthermore, processing PDAC patient samples according to the continuum sorting approach revealed that the majority of PDAC samples contain CTCs that were categorized at all three expression levels, with the majority of CTCs

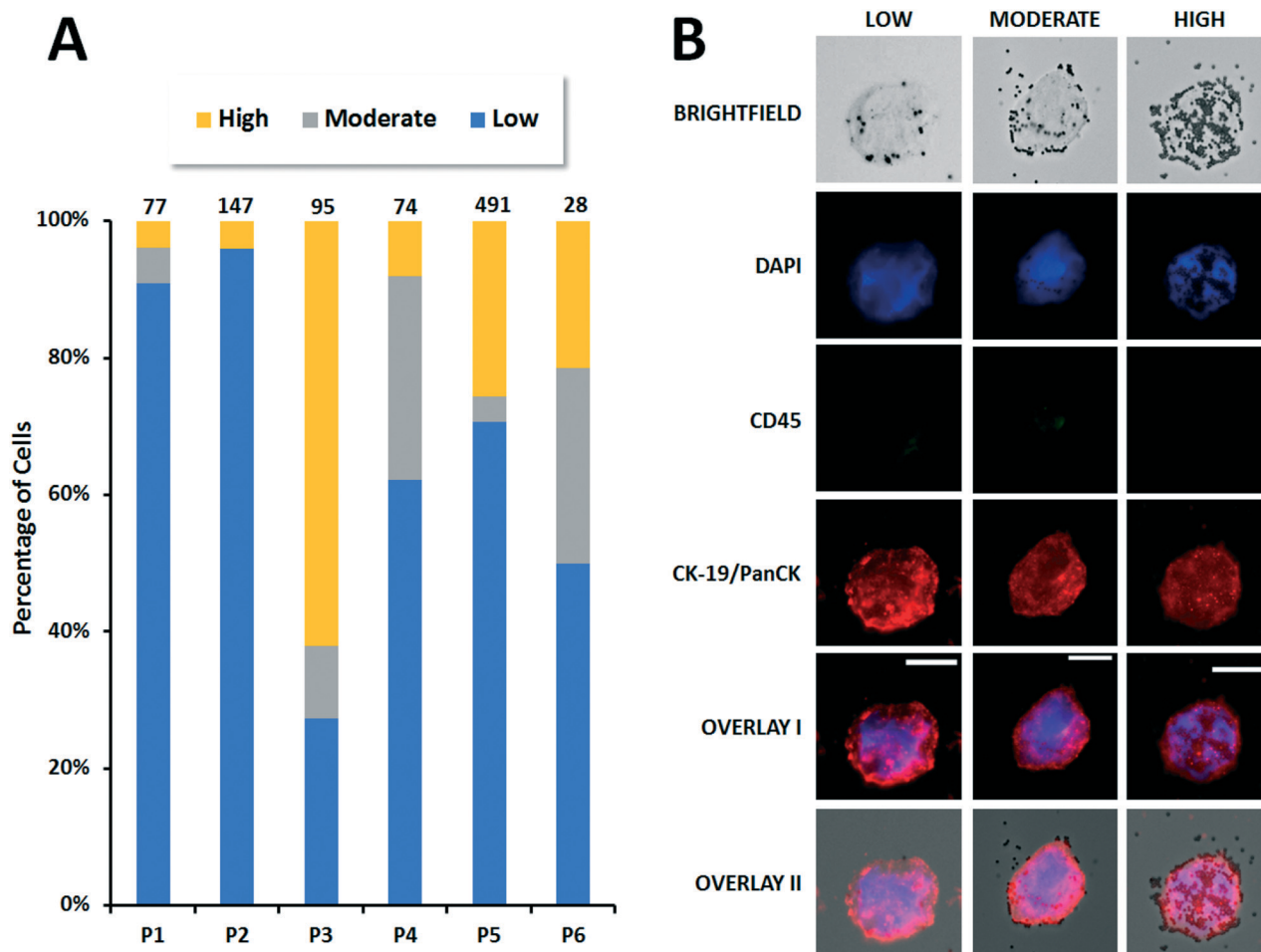


Fig. 5 Continuum isolation of PDAC CTC (A) percentage of CTCs isolated according to low, moderate and high EpCAM levels. CTCs per mL for each patient is indicated above bar. (B) Brightfield and immunofluorescent images of CTCs isolated based on low, moderate and high EpCAM expression levels (scale bars represent 20 μ m).

expressing low levels of EpCAM. We have demonstrated a sensitive and reproducible approach to isolate cancer cell populations according to a continuum of surface protein expression levels and demonstrated the clinical relevance of the system *via* CTC isolation. The work represents a step towards studying the continuum of tumor cell heterogeneity in a clinically meaningful manner.

Acknowledgements

This research was funded by DOD-CDMRP-PCRP Concept Award W81XWH-12-PCRP-CDA to S. Nagrath. We thank H. Cameron for patient sample retrieval. We also thank the Lurie Nanofabrication Facility, a member of the National Nanotechnology Infrastructure Network (NNIN) funded by the National Science Foundation for use of equipment to fabricate devices.

References

- 1 D. A. Landau, *et al.*, Evolution and Impact of Subclonal Mutations in Chronic Lymphocytic Leukemia, *Cell*, 2013, **152**, 714–726.
- 2 E. A. Mroz and J. W. Rocco, MATH, a novel measure of intratumor genetic heterogeneity, is high in poor-outcome classes of head and neck squamous cell carcinoma, *Oral Oncol.*, 2013, **49**, 211–215.
- 3 J. Zhang, *et al.*, Intratumor heterogeneity in localized lung adenocarcinomas delineated by multiregion sequencing, *Science*, 2014, **346**, 256–259.
- 4 N. McGranahan and C. Swanton, Biological and Therapeutic Impact of Intratumor Heterogeneity in Cancer Evolution, *Cancer Cell*, 2015, **27**, 15–26.
- 5 J. Calbo, *et al.*, A Functional Role for Tumor Cell Heterogeneity in a Mouse Model of Small Cell Lung Cancer, *Cancer Cell*, 2011, **19**, 244–256.
- 6 P. L. Bedard, A. R. Hansen, M. J. Ratain and L. L. Siu, Tumour heterogeneity in the clinic, *Nature*, 2013, **501**, 355–364.
- 7 J. Castle, H. Shaker, K. Morris, J. D. Tugwood and C. C. Kirwan, The significance of circulating tumour cells in breast cancer: A review, *Breast*, 2014, **23**, 552–560.
- 8 N. Aceto, *et al.*, Circulating tumor cell clusters are oligoclonal precursors of breast cancer metastasis, *Cell*, 2014, **158**, 1110–1122.
- 9 C. A. Klein, *et al.*, Genetic heterogeneity of single disseminated tumour cells in minimal residual cancer, *Lancet*, 2002, **360**, 683–689.
- 10 D. T. Ting, *et al.*, Single-cell RNA sequencing identifies extracellular matrix gene expression by pancreatic circulating tumor cells, *Cell Rep.*, 2014, **8**, 1905–1918.
- 11 A. S. Cleary, T. L. Leonard, S. A. Gestl and E. J. Gunther, Tumour cell heterogeneity maintained by cooperating subclones in Wnt-driven mammary cancers, *Nature*, 2014, **508**, 113–117.
- 12 A. Boiko, Isolation of Melanoma Tumor-Initiating Cells from Surgical Tissues in *Molecular Dermatology*, ed. C. Has and C. Sitaru, Humana Press, 2013, vol. 961, pp. 253–259.
- 13 K. J. Cheung, *et al.*, Polyclonal breast cancer metastases arise from collective dissemination of keratin 14-expressing tumor cell clusters, *Proc. Natl. Acad. Sci. U. S. A.*, 2016, **113**, E854–E863.
- 14 M. C. Chang, Y. T. Chang, J. Y. Chen, Y. M. Jeng, C. Y. Yang, Y. W. Tien, S. H. Yang, H. L. Chen, T. Y. Liang, C. F. Wang, E. Y. Lee, Y. C. Chang and W. H. Lee, *Clin. Chem.*, 2016, **62**, 505–513.
- 15 R. M. Mohamadi, *et al.*, Nanoparticle-Mediated Binning and Profiling of Heterogeneous Circulating Tumor Cell Subpopulations, *Angew. Chem., Int. Ed.*, 2015, **54**, 139–143.
- 16 R. M. Jack, *et al.*, Ultra-Specific Isolation of Circulating Tumor Cells Enables Rare-Cell RNA Profiling, *Adv. Sci.*, 2016, **3**, 1600063.
- 17 S. D. Wit, *et al.*, The detection of EpCAM+ and EpCAM–circulating tumor cells, *Sci. Rep.*, 2015, **5**, 12270.
- 18 C. Derec, C. Wilhelm, J. Servais and J.-C. Bacri, Local control of magnetic objects in microfluidic channels, *Microfluid. Nanofluid.*, 2009, **8**, 123–130.
- 19 G. Kokkinis, F. Keplinger and I. Giouroudi, On-chip microfluidic biosensor using superparamagnetic microparticles, *Biomicrofluidics*, 2013, **7**, 054117.
- 20 T. Schneider, *et al.*, Sequential CD34 cell fractionation by magnetophoresis in a magnetic dipole flow sorter, *Analyst*, 2010, **135**, 62–70.
- 21 M. G. Lampugnani, Cell migration into a wounded area in vitro, *Methods in molecular biology*, ed. N. J. Clifton, 1999, vol. 96, pp. 177–182.
- 22 Y. Chen, *et al.*, Combined integrin phosphoproteomic analyses and small interfering RNA-based functional screening identify key regulators for cancer cell adhesion and migration, *Cancer Res.*, 2009, **69**, 3713–3720.